Journal of the Energy Institute 100 (2022) 189–196

Contents lists available at ScienceDirect

Journal of the Energy Institute

journal homepage: www.elsevier.com/locate/joei

Effect of coke ratio on pore structure evolution in the high-temperature zone of sintering bed

Hao Zhou *, Hanxiao Meng, Pengnan Ma, Jiankang Wang

State Key Laboratory of Clean Energy Utilization, Institute for Thermal Power Engineering, Zhejiang University, Hangzhou, 310027, PR China

ARTICLE INFO

Keywords:
Iron ore sintering
Coke ratio
High-temperature zone
Pore structure

ABSTRACT

The high-temperature zone of the sintering bed is the crucial area for material change and structural remodeling, and the heat is provided by coke combustion. Understanding how fuel combustion affects bed structure is of great significance to optimize sintering parameters and sintering quality. In this study, sintering pot tests were carried out under three coke ratios of 4.5%, 5.0% and 5.5%, and liquid nitrogen was used to quench the high-temperature zone sintering. The clear internal structure of the high-temperature zone sinter was obtained using X-ray computed tomography (XCT). Results show that with the increase of coke ratio, the porosity in the high-temperature zone decreases from 54.29% to 51.04% and 48.07%, and the number of terminal nodes, branch nodes and segments of the pore skeleton decreases by 51.6%, 55.2% and 53.1% respectively. The pores in the high-temperature zone are fully fused and developed.

1. Introduction

With the increasingly severe ecological and climate problems caused by global warming, carbon emission reduction has become one of the focuses of development and research in many industries [1]. As a developing country, a large part of carbon emissions in China come from secondary industry, especially the combustion process of fossil fuels [2]. As an energy-intensive industry, the carbon emission of the iron and steel industry deserves special attention [3]. The statistical results show that in 2018, the total CO_2 emissions from smelting and pressing of ferrous metals processes in China reached 1769.6 million tons (Mt), accounting for 18.4% of the total national emissions, including 1068.7 Mt from coke combustion, which accounts for 60.4% of the emissions from the welding and pressing of ferrous metals process [4]. As an ore powder agglomeration method widely used globally, the importance of the sintering process for the quality and output of iron and steel smelting cannot be overemphasized [5], which accounts for more than 10% of the total energy consumption of the iron and steel industry. Thus, optimizing energy utilization in the sintering process is of great significance to carbon emission reduction in the steel industry.

The sintering process of iron ore is a self-sustaining porous medium combustion process of a packed bed formed after granulation of a certain proportion of ores, fluxes, fuel and return fines under negative pressure suction after ignition [6]. Coke is widely used as sintering fuel in industry, also the primary source of carbon emissions [7]. The sintering bed was usually stratified according to its temperature and moisture in previous studies [8,9]. The igniter ignites the sintering bed to form a flame front, and then the combustion of coke maintains the flame front. That is, a high-temperature zone gradually propagating downward is formed [10]. On the one hand, the addition amount, combustion speed and rate of coke determine the propagation speed of the flame front, the width and the temperature of the high-temperature zone [11,12], which further affect the evolution of the sintering bed structure [13], sinter quality and yield [14] and the flue gas composition [15]. On the other hand, coke consumption and combustion are the decisive factors of carbon emission in the sintering process [4].

The application effect and combustion characteristics of various forms of fuel have been thoroughly studied. The combustion behavior of coke breeze at different particle sizes and its effect on sintered products have been widely studied [16,17]. Besides, Fan et al. investigated the effect on ignition parameters and the optimization on sintering quality of coke segregation [18]. The combustion behaviors of different types of quasi-particles obtained by changing the coke distribution through the change of granulation process have been also studied [17,19,20]. The effects of coke distribution on sintering parameters, sintering quality, and sintering flue gas composition have also been thoroughly discussed and verified by experiments [21–24]. It is also one of the research hotspots in recent years to reduce fossil energy consumption and the

* Corresponding author.
E-mail address: zhouhao@zju.edu.cn (H. Zhou).

https://doi.org/10.1016/j.joei.2021.11.014
Received 13 September 2021; Received in revised form 18 November 2021; Accepted 25 November 2021
Available online 29 November 2021

emission of flue gas pollutants by replacing coke with biomass fuel in different proportions [25,26]. However, biomass fuel is often more reactive and burns faster. Therefore, many laboratory studies use flux powder or ore powder to pre-granule biomass fuel to form coated quasi-particles [20,27]. Similarly, the modification of biomass fuel by impregnation is also to improve its combustion characteristics and meet the needs of the sintering process [20,28].

However, the bed structure is constantly evolving in the sintering process, mainly in the high-temperature zone and driven by the airflow impact and the heat release of coke combustion [29]. The traditional analysis of bed structure mainly measures green bed bulk density, permeability, and sintered bed porosity [13]. The porosity of sinter measured by traditional methods such as mercury intrusion porosimetry does not include closed pores [30], while optical microscopy can not effectively count the volume and quantity of large pores [31]. X-ray computed tomography (XCT) is a non-destructive visualization technology for the internal three-dimensional (3D) structure of objects., which has played a significant role in the structural research of porous media in recent years [32,33]. Nushiro et al. [34] have already used XCT to analyze the structure and density of the sinter but can not obtain many accurate and compelling data, limited by the resolution and data processing capacity of the equipment at that time. With the improvement of XCT accuracy and the development of image processing technology, it is not difficult to effectively distinguish whether the pores in the sinter are open or closed [30]. Furthermore, Zhou et al. calculated the permeability of raw material bed and sintering bed after obtaining the pore structure of the green bed and sintering bed with XCT [35,36] and put forward the calculation method of effective thermal conductivity of sinter [37], combined with computational fluid dynamics (CFD). XCT can also help to analyze the strength properties of green bed or sintering bed [38,39].

What is more, the pressure drop in the high-temperature zone is the controlling factor of the overall pressure drop of the sintering bed, which is mainly affected by the temperature and structure of the high-temperature zone, and further affects the sintering speed and sintering quality [8,11]. Clarifying the impact of coke combustion on the sintering process, so as to determine the appropriate amount and mode of coke addition, has guiding significance for carbon emission reduction in the sintering process and the improvement of sintering product quality. However, it is difficult to obtain complete samples of the changing high-temperature zone bed during sintering, so few studies show how fuel combustion affects the evolution of bed structure in the high-temperature zone. Liquid nitrogen was used to quench the sintering bed to obtain complete sinter samples in the high-temperature zone in this study. Then the 3D structure of the samples was reconstructed by XCT, and the visualization of the sintering bed structure in the change process can be realized. The pore quantity and morphological characteristics of sinter in high-temperature zone with different coke ratio were analyzed, and the influence mechanism of coke combustion process on bed structure evolution was clarified, providing a valuable reference for exploring the methods to improve the quality and output of sinter.

2. Experimental and materials

2.1. Sinter pot tests

The pilot-scale sinter pot tests in this study were as close to the industrial operation as possible to ensure that the experimental results have better reference significance for industrial production. A typical ore batching in the Asia Pacific region is adopted, including three ores from Australia and two Brazil, as shown in Table 1. The binary basicity was set to 1.90 by controlling the addition of limestone and dolomite as fluxes, appropriate for the sinter quality according to our previous researches using the same ores [40,41]. The return fines ratio was controlled at 25% by adding return fines with particle sizes of 0–3.35 mm and 3.35–5 mm to the raw materials in the ratio of 1:2, referring to the engineering experience. Three sinter pot tests with the coke ratio of 4.5 wt%, 5.0 wt% and 5.5 wt% on dry basis were conducted to evaluate the effect of the coke ratio on the flame front propagation and provide samples for the study of pore structure.

Table 1
Ore blend proportion and sintering conditions.

Ore blend proportion (wt.% ore basis)		
Ore 1 from Australia	16.67	
Ore 2 from Australia	16.67	
Ore 3 from Australia	33.33	
Ore 4 from Brazil	16.67	
Ore 1 from Brazil	16.67	
Sintering conditions		
Basicity	1.9	
Return fines ratio (wt.% total basis)	25	
Bed height (mm)	650	
Ignition suction (kPa)	6	
Ignition temperature (°C)	1200	
Ignition time (s)	90	
Sintering suction (kPa)	16	
Coke ratio (wt.% total basis)	Case1	4.5
	Case2	5.0
	Case3	5.5

The schematic diagram of the sinter pot tests device is shown in Fig. 1. The raw materials weighted according to Table 1 were hoisted into the drum for 1 min dry mix. An automatic feeding chute then fed the mixed materials to a bigger drum for 10 min granulation by adding water as a target moisture content of 6.35% of the total weight for all cases. 1 kg sinters with a particle size of 6.3–8 mm were paved at the bottom of the sinter pot with a height of 650 mm and an inner diameter of 120 mm advance to ensure the air permeability of the bed under the premise of no leakage. The granulated raw materials were then filled into the sinter pot. The samples were taken from the remaining granulation, weighed and placed in the oven. The moisture content of raw materials was calculated by the mass difference before and after drying, and then the working conditions deviating from the target moisture were repeated. Table 1 shows the sintering conditions. Six pressure transmitters are installed at five different heights of the bed and the outlet of the wind box respectively, as shown in Fig. 1. The sharp decrease of bed negative pressure means the passage of the flame front. It indicates that the sintering is about half-finished when the bed negative pressure at 300 mm from the top of the sinter pot decreases rapidly. At this time, the induced draft fan was turned off, and liquid nitrogen was rapidly injected to quench the bed. The high-temperature zone where materials coagulation and structural evolution were taking place was rapidly cooled and the shape fixed.

2.2. XCT imaging and post-processing process

The size of the sinter fed into the blast furnace in the industrial ironmaking process is generally 5–40 mm, and the scale of the XCT system limits the size of the sample. So 100 × 100 mm cylindrical samples in high-temperature zone sinter obtained by liquid nitrogen quenching after sintering were taken out to visualize the internal structure, which is sufficient to include the main structural characteristics of sinter. The samples were fixed on the precision sample platform of the XCT device as shown in Fig. 2 for imaging. The selection of appropriate imaging parameters is essential before XCT imaging operation. Too low the resolution of the XCT unit will result in the inability to recognize the small-scale geometric features inside the sinter, while too high resolution will lead to a large amount of imaging data and consume a lot of computing resources for processing. In most studies related to the pore structure of the sinter, pores larger than 1 mm are usually called “macropore”, otherwise they are called “micropore” [40]. Weighing the accuracy requirements of the analysis and the computing power of the

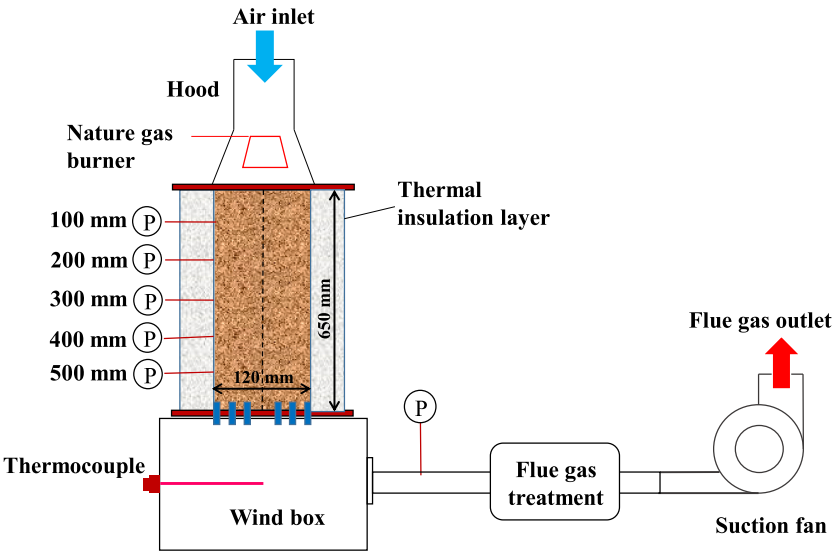

Fig. 1. Schematic representation of the sinter pot system.

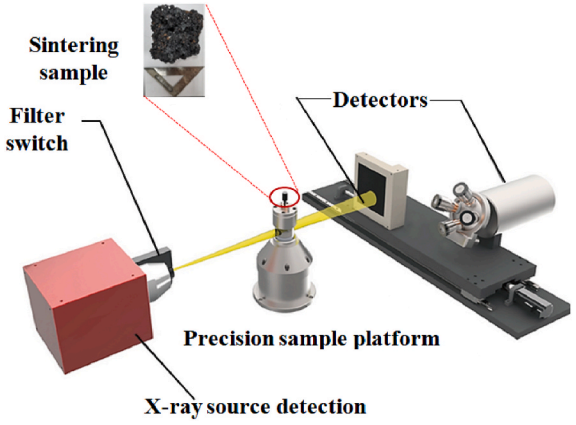

Fig. 2. X-ray computed tomography system for sintering sample.

server, the imaging resolution was set to 74 μm. Other parameters of the XCT system are shown in Table 2.

Slice grayscale image inside sinter was obtained utilizing the XCT imaging process, as shown in Fig. 3 (a). Obviously, the larger the region of interest, the more representative the statistical results of pore characteristics are. However, it consumes a lot of calculation resources to reconstruct the three-dimensional structure of sinter and analyze the pore characteristics through XCT data. In view of the 1 mm pore size limit of "macropore" and "micropore" mentioned above and our preliminary

Table 2
Parameter setting of XCT system.

Parameter	Unit	Value
Voltage	kV	190
Current	μA	350
Exposure time	s	0.8
Distance from X-ray source to sample	mm	510
Distance from detector to sample	mm	860
Resolution	μm	74

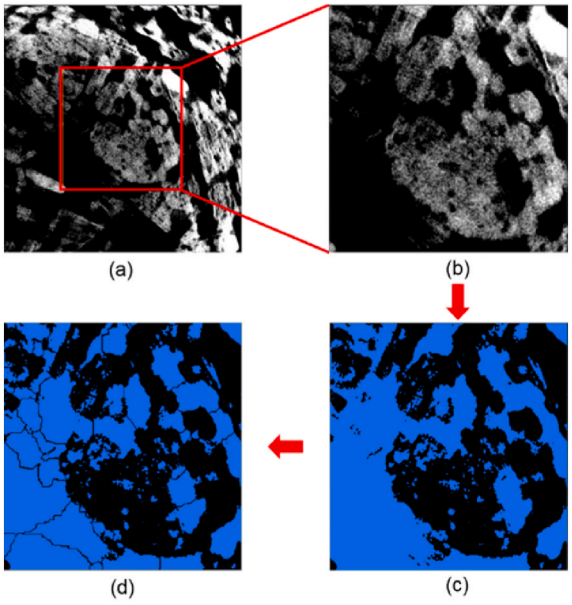

Fig. 3. XCT images processing procedure: (a) original grayscale image; (b) selection (ROI); (c) noise reduction and binarization; (d) segmentation.

reconstruction, we chose a 30 × 30 × 30 mm^3 cube region as the region of interest (ROI), which is sufficient to provide the required sinter structural characteristics and reduce the calculation time as much as possible within the scope of our server, as shown in Fig. 3 (b). The noise reduction and binarization of the grayscale image can make the boundaries of the solid phase (blue) and pores (black) clear, as shown in Fig. 3 (c). Finally, the binary slices were segmented to count the shape and distribution characteristic parameters of pores as shown in Fig. 3 (d).

The main pore shape parameters include equivalent diameter (D_e) and sphericity (Ψ), calculated according to the following equations (1) and (2).

$$D_e = \sqrt[3]{\frac{6V}{\pi}} \quad (1)$$

$$\psi = \frac{\sqrt[3]{\pi(6V)^2}}{S} \quad (2)$$

Where V is the volume of pores (m^3), and S is the area of pores (m^2).

3. Results and discussion

3.1. Effect of coke ratio on flame front propagation

During the sintering process, the suction of the induced draft fan makes the whole bed in a negative pressure state. The closer to the bottom of the sintering cup, the higher the bed negative pressure of the bellows. As sintering proceeds, the flame front moves downward. The bed where the flame front has passed is the sintered zone, and the area where the flame front has not reached is the unsintered zone or raw material zone. Fig. 4 shows the distribution and change of sintering bed pressure during sintering under different coke ratio conditions. The results show that the decrease time of bed negative pressure is slightly delayed with the increase of coke ratio from 5.0% to 5.5%, which indicates that the vertical sintering speed becomes slower.

On the one hand, in the case of a high coke ratio, fuel combustion will release more heat, resulting in higher bed temperature and more melt formation. The gas in the high-temperature zone will expand and increase the gas flow resistance. The higher the temperature, the stronger the expansion and the greater the resistance. The formation of melt is conducive to the agglomeration of materials and the remodeling of the sinter structure. However, too much melt may block the gas flow channels in the high-temperature zone in a short time, resulting in the obstruction of the downward heat transfer of the gas flow in the high-temperature zone. On the other hand, more coke combustion requires more oxygen. In the rapid combustion process in the high-temperature zone, the oxygen in the gas flow is rapidly consumed and the oxygen potential is rapidly reduced, resulting in slower coke combustion and slower flame front propagation. However, the gas flow is easier to overcome the resistance of the liquid phase and form channels when the gas flow driving force caused by the negative pressure of the bellows is large according to our previous study [8]. Therefore, the increase of melt caused by high coke ratio has no obvious effect on the deceleration of gas flow velocity under high bellows negative pressure, which explains that the effect of the increase of coke ratio on the slowing down of sintering speed is not too apparent under the negative pressure of 16 kPa bellows used in this study.

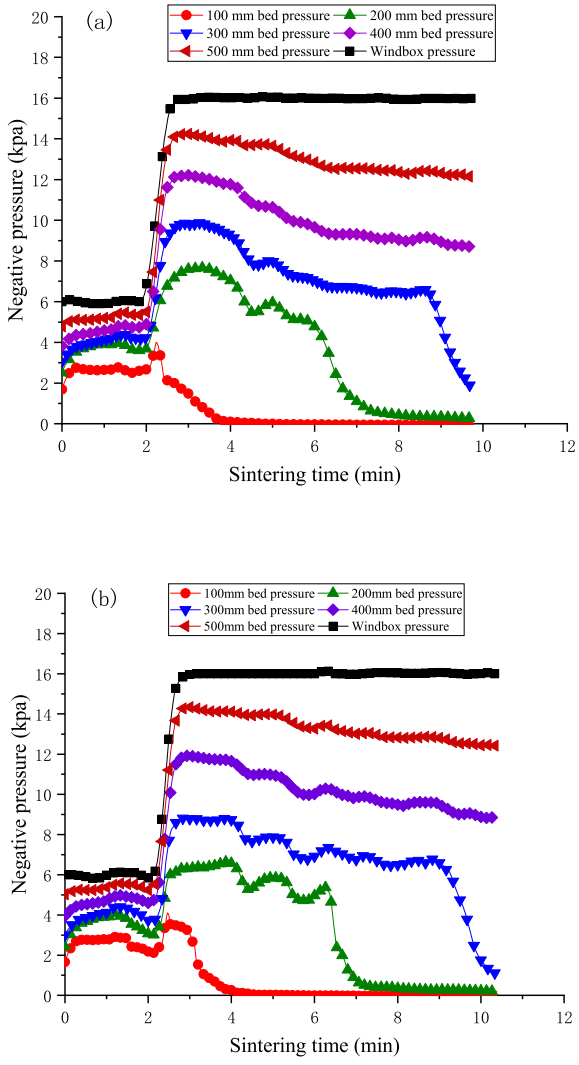

Fig. 4. Change of negative pressure of sintering bed under different coke ratio (a)5.0%, (b)5.5%.

3.2. Pore distribution characteristics in the high-temperature zone

The green bed is filled with granulated sintering raw materials. A series of physical and chemical reactions occur in the sintering process, especially in the high-temperature zone. The heat released by fuel combustion makes the bed temperature in the high-temperature zone reach more than 1200 °C, and the fine powder adhesion layer of quasi-particles melts to liquid phase. The liquid phase flows under the influence of viscous force, surface tension and gravity to connect the initially dispersed granulation. At the same time, the original voids between quasi-particles gradually penetrate under the impact of gas flow to form channels. With heat transfer front and flame front propagation during sintering, the high-temperature zone gradually shifts downward. The original high-temperature zone gradually cooled down. The solidified liquid phase binds the granules to form agglomerated sinter, and the bed structure is remolded.

The distribution of solid matrix, pores and closed pores in the high-temperature zone are shown in Fig. 5. With the increase of coke ratio from 4.5% to 5.0% and 5.5%, the porosity in the high-temperature zone is 54.29%, 51.04% and 48.07% respectively. The solid matrix shows a trend from granular to cohesive. More heat is released at a higher coke ratio, which is conducive to the formation of the molten liquid phase. As discussed above, a high coke ratio brings high bed temperature, more molten liquid phase generation and long sintering time, promoting the melting and coagulation of sintering materials. Therefore, the bed structure is fully remolded, the degree of solid matrix integration is higher, and the porosity of sinter is lower under higher coke ratio conditions.

In order to characterize the pore distribution more intuitively, we counted the changes of surface porosity in three directions in space, as shown in Fig. 6. It can be seen from Figs. 6 and 5 that the number and size of pores are random and disordered in each direction. The granulation and filling of sintering raw materials form an anisotropic green bed stacking structure. The high temperature remodeling of the bed and the impact of gas flow in the sintering process do not change the anisotropy of the bed structure.

3.3. Pore morphological characteristics in the high-temperature zone

Fig. 7 shows the pore frequency distribution according to equivalent diameter under different coke ratios. The pores of 0–0.2 mm account for more than 40% of the total number, and the pores of 0–0.4 mm account for more than 70%. Under any conditions, the pores larger than 1 mm account for no more than 13%. Fig. 8 shows the pore volume fraction according to equivalent diameter under different coke ratios. The pore volume fraction of pores larger than 3 mm is about 90%, while that of

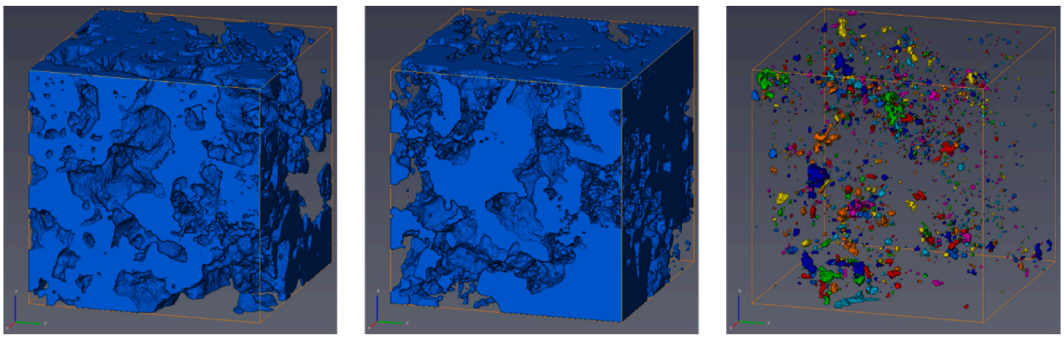

(a) 4.5%

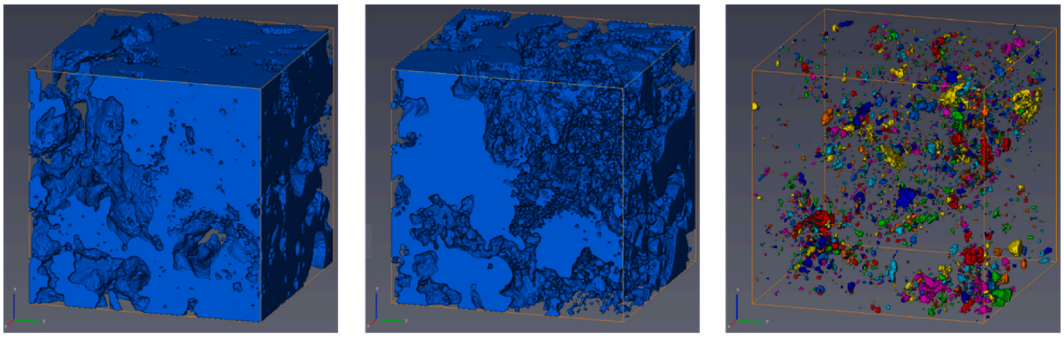

(b) 5.0%

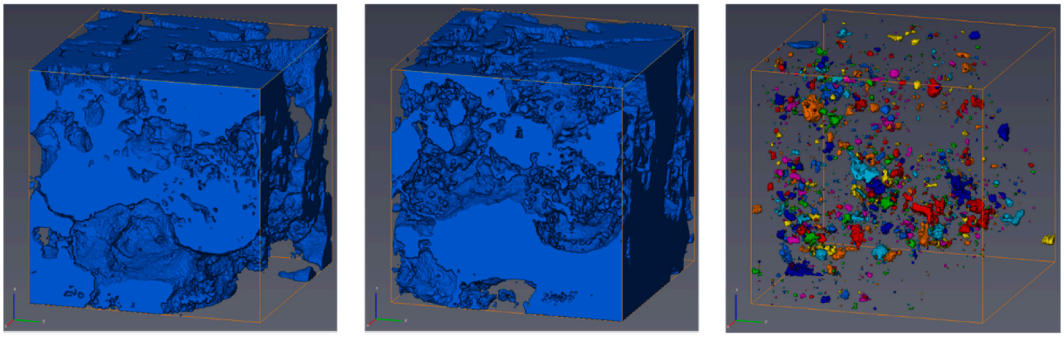

(c) 5.5%

Fig. 5. Distribution of matrixes and pores (left: solid matrix, middle: pore structure, right: closed pores).

pores larger than 1 mm is about 99%. It can be seen that the number frequency distribution and volume fraction distribution of pores with different sizes are basically the same. Although the number of micropores accounts for the vast majority, its volume fraction is almost negligible, which greatly impacts the strength and metallurgical characteristics of the sinter but not on the gas flow channels. The dominant macropores in volume fraction dominate the permeability in the high-temperature zone.

In the process of sintering the flame front propagating downward, a complex three-phase merger of solid phase, melting and bubbles happen in the high-temperature zone. The shape of bubbles is constantly changing. Fig. 9 shows the sphericity of pores of various sizes at different coke ratios. Obviously, the smaller the pore size, the greater its sphericity, that is, the closer it is to a sphere. The bubble in the high-temperature zone is a region surrounded by the interface between the molten liquid phase and gas. Surface tension takes $2\gamma/r$ as the driving force to promote the remodeling of bubbles to the form with low system energy to make its state stable, where r is the bubble radius. While the viscosity of the liquid phase will prevent this remodeling process [42]. The smaller the bubble, the greater the effect of surface tension, and the easier the bubble is to reshape to the sphere, which is the form with low system energy.

It can also be seen from Fig. 9 that the sphericity of pores in a specific size range tends to increase with the increase of the coke ratio. The pore sphericity under the 5.5% coke ratio condition is greater than that under the other two conditions. On the one hand, under the condition of a high coke ratio, the bed temperature is high, the amount of liquid phase is increased, and its viscosity is low. The resistance of viscous force to pores remodeling process is reduced. On the other hand, a slow combustion rate under a high coke ratio means a long holding time of the high-temperature zone. There is more time for the bubble to develop into a nearly spherical shape driven by surface tension. In the process of liquid nitrogen quenching, the evolving bubbles are frozen instantaneously to obtain more spherical pores at a high coke ratio.

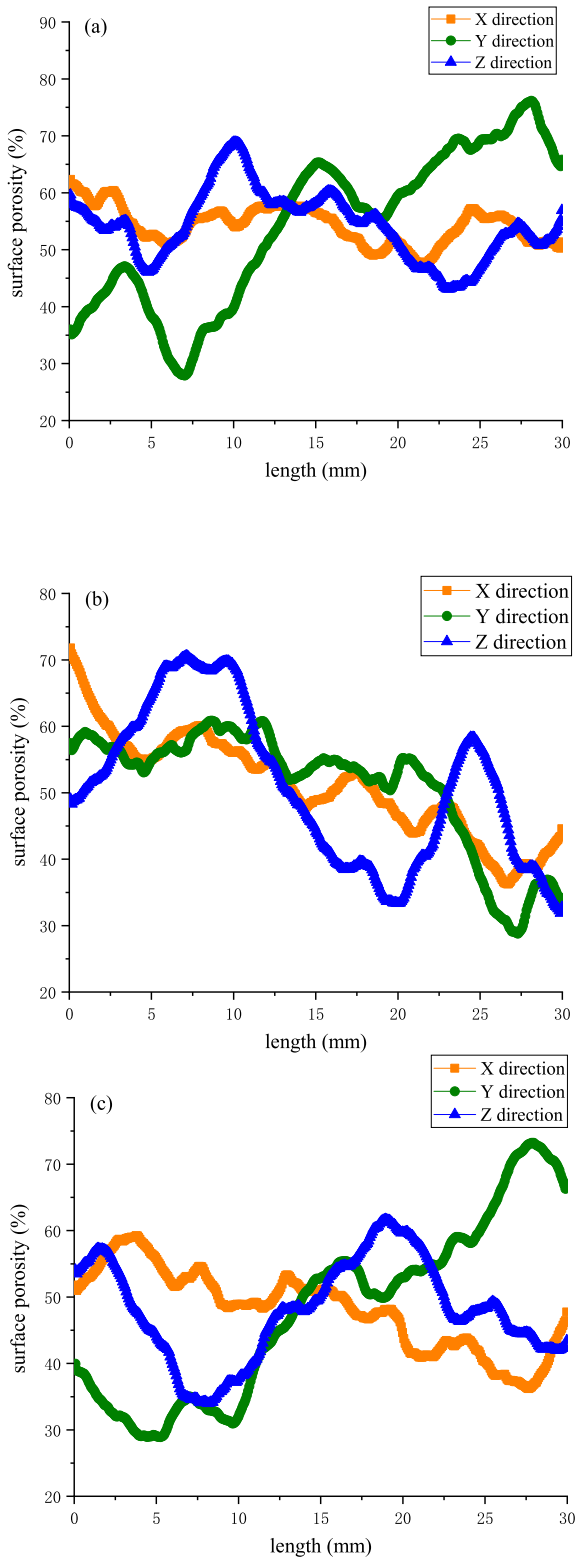

Fig. 6. Surface porosity in different directions under different coke rate, (a) 4.5%, (b) 5.0%, (c) 5.5%.

3.4. Pore skeleton network and parameters

The centerlines of the interconnection region are extracted from the interior of the porous structure, and the size of each section of the centerline is expanded according to the pore size of each region, so as to obtain the pore skeleton network. The extraction of the pore skeleton

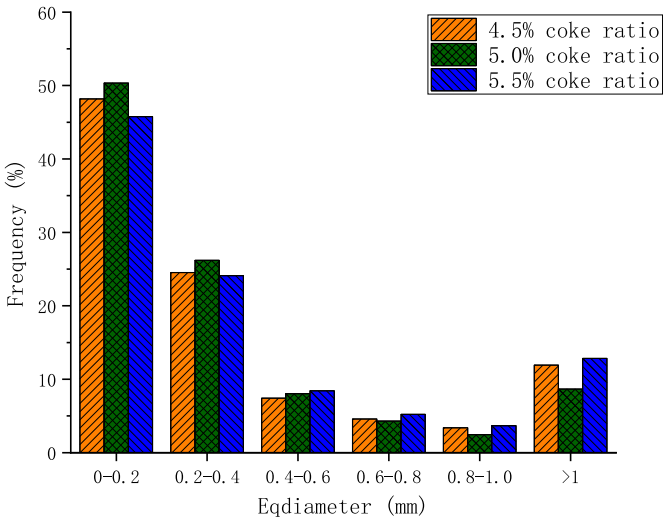

Fig. 7. Frequency distribution of pores with different sizes.

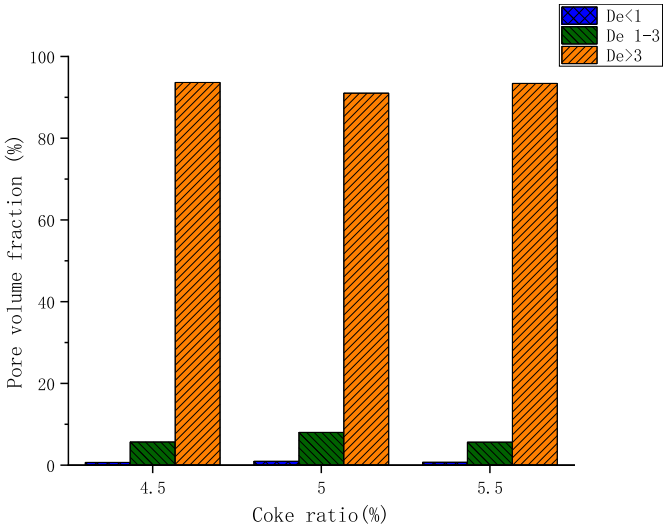

Fig. 8. Volume fraction of pores with different sizes under different coke ratio.

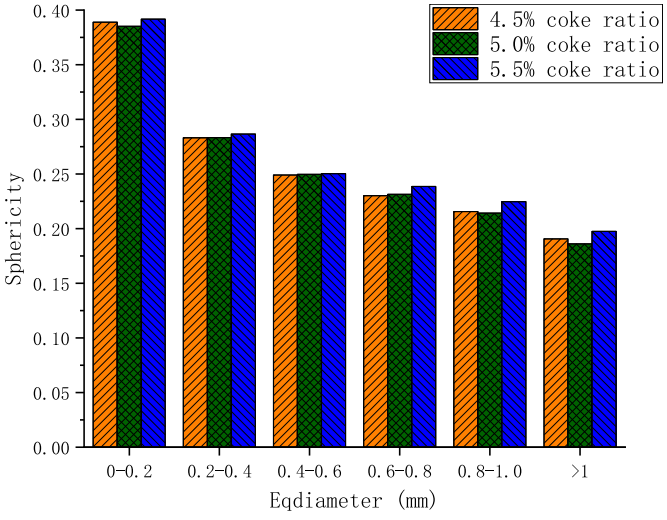

Fig. 9. Sphericity of pores with different sizes under different coke rate.

network is helpful to visually characterize the shape and distribution of annual connected pores in the high-temperature zone and carry out the parametric analysis. As shown in Fig. 10, the pores gradually develop close to the channels impacted by the gas flow. But the distribution of pore skeleton under different coke ratios is random, and the length, radius and shape of pores are obviously uneven. A pore may gradually develop into several branches or end somewhere.

The position where the pore branches is called the branching node, the end of the pore is called the terminal nodes, and the pore part between two adjacent nodes is called the segment. The detailed parameters of the pore skeleton are statistically analyzed in Fig. 11. With the increase of the coke ratio, the total volume and total length of the pore framework decrease, which is consistent with the changing trend of porosity in the high-temperature zone in Section 3.2. In addition, it can be seen that the increase of the coke ratio has a more significant impact on the total length of the pore skeleton than on the total volume. With the increase of coke ratio from 4.5% to 5.5%, the total volume of pore skeleton decreases by 11.5%, while the total length decreases by 25.3%.

On the one hand, the lower liquid phase viscosity and longer sintering time under a high coke ratio make the materials fully integrate. Some small bubbles merge into large bubbles and break out from the liquid phase, reducing total pores volume in the high-temperature zone. On the other hand, the connected pores in a large number of low viscosity liquid phases are easier to expand and coarsen due to the expansion of internal gas at high temperature, forming relatively short and coarse gas flow channels, which also confirms the influence law of coke ratio on pore sphericity.

Fig. 11 (b) shows that with the increase of coke ratio, the number of terminal nodes, branching nodes and segments of the pore skeleton all decrease significantly. The reduction rates were 51.6%, 55.2% and 53.1% respectively as the coke ratio increase from 4.5% to 5.5%, obviously higher than the reduction of total volume and total length of the pore skeleton. This shows that the more sufficient pore fusion and development not only leads to the relatively short and thick pore skeleton, but also makes the segments of the pore skeleton longer or less branched. This is because the long holding time of the high-temperature zone makes the bubbles more likely to contact each other, so that the two terminal nodes merge and fuse to form a more extended segment. Low liquid viscosity leads to easy expansion and coarsening of bubbles. In this process, some tiny branches may be swallowed by the trunk, and the branching nodes and their corresponding segments disappear. In addition, it can be seen from Fig. 10 that very few pore segments do not branch or only branch one or two. Therefore, the relative relationship that the number of terminal nodes is less than the number of branching nodes and less than the number of segments is well understood.

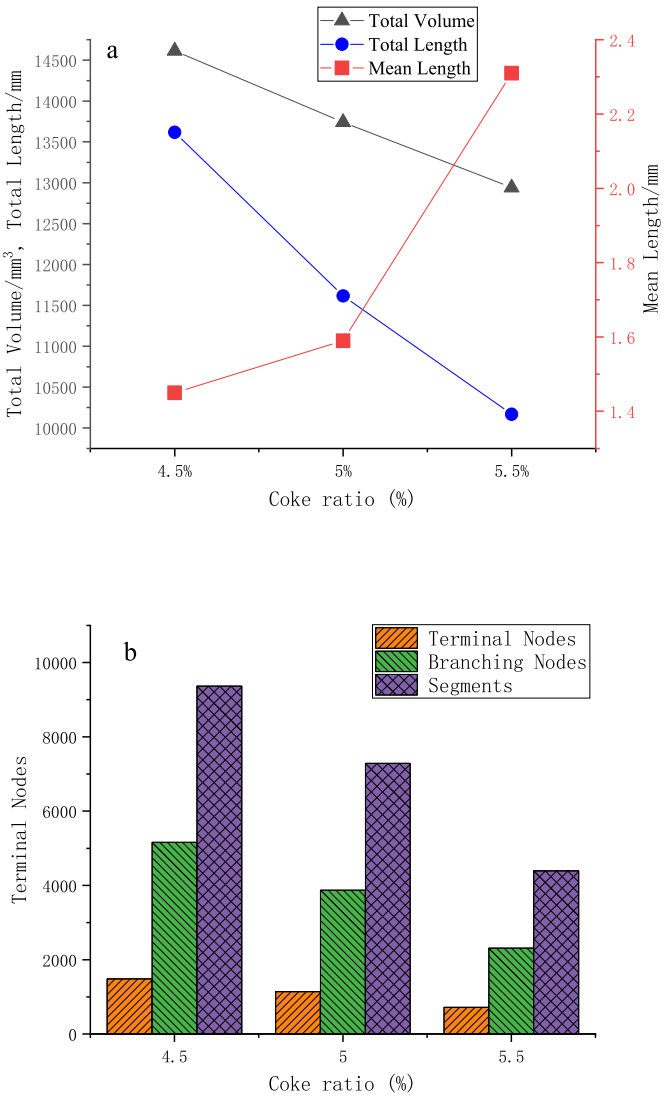

Fig. 11. Comparison of pore skeleton parameters under different coke ratios.

4. Conclusions

In order to study the influence of coke ratio on the structural evolution of high-temperature zone in the sintering process, sintering pot tests under three coke ratio conditions were carried out, then the high-temperature zone being sintered was quenched with liquid nitrogen. The three-dimensional structure of the high-temperature zone of the sintering bed was reconstructed using XCT. By analyzing the sintering and XCT data, the following main conclusions are obtained:

1. High coke ratio leads to violent gas expansion and more melt formation in the high-temperature zone, significant gas flow resistance in the high-temperature zone, lower oxygen potential and slower coke combustion, thus slowing down the sintering speed.

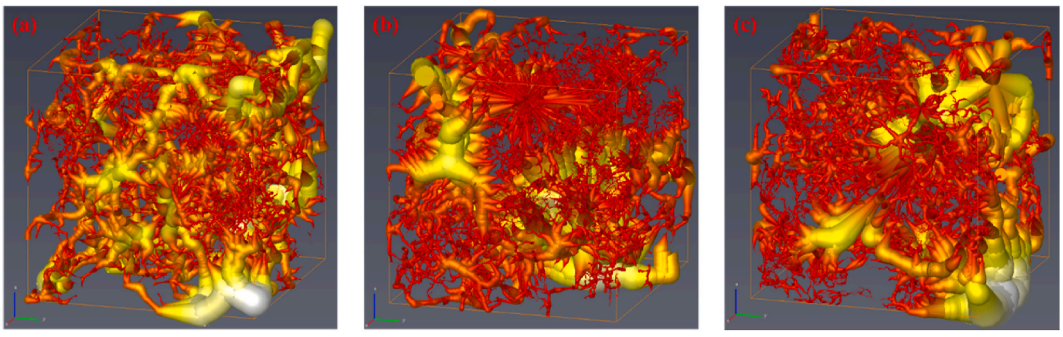

Fig. 10. Pore framework network under different coke rate (a)4.5%, (b)5.0%, (c)5.5%.

2. As the coke ratio increases from 4.5% to 5.0% and 5.5%, the bed materials are fused more fully, the solid matrix in the high-temperature zone changes from granular to bonded, and the porosity decreases from 54.29% to 51.04% and 48.07%.
3. Increasing the coke ratio can improve the sphericity of pores in the high-temperature zone and promote the remolding of the pore network. The number of terminal nodes, branching nodes and segments of the pore skeleton decrease by 51.6%, 55.2% and 53.1%, respectively.

Declaration of competing interest

The authors declare no conflicts of interest.

Acknowledgment

Funding: This work was supported by National Natural Science Foundation of China [grant number 52036008].

References

[1] T. Nakazawa, Current understanding of the global cycling of carbon dioxide, methane, and nitrous oxide, Proc. Jpn. Acad. Ser. B Phys. Biol. Sci. 96 (2020) 394–419, https://doi.org/10.2183/pjab.96.030.
[2] L. Li, W. Xue, Iop, Carbon Emissions Influence Factors and Peak Forecast Study of China, 2nd International Conference on Air Pollution and Environmental Engineering (APEE)Xian, 2019, https://doi.org/10.1088/1755-1315/450/1/012095. PEOPLES R CHINA.
[3] J. Zhao, H. Zuo, Y. Wang, J. Wang, Q. Xue, Review of green and low-carbon ironmaking technology, Ironmak. Steelmak. 47 (2019) 296–306, https://doi.org/10.1080/03019233.2019.1639029.
[4] CEADs (China Emission Accounts and Datasets), Emission Inventories by Sectoral Approach, 2018. https://www.ceads.net.cn/data/nation/.
[5] H. Zhou, J.P. Zhao, C.E. Loo, B.G. Ellis, K.F. Cen, Numerical modeling of the iron ore sintering process, ISIJ Int. 52 (2012) 1550–1558, https://doi.org/10.2355/isijinternational.52.1550.
[6] D. Fernández-González, I. Ruiz-Bustinza, J. Mochón, C. González-Gasca, L. F. Verdeja, Iron ore sintering: process, Miner. Process. Extr. Metall. Rev. 38 (2017) 215–227, https://doi.org/10.1080/08827508.2017.1288115.
[7] A. Kojo Alex, W. Shijie, H. Fang, X. Wu, W. Chen, P. Che, Z. Xu, Review on alternative fuel application in iron ore sintering, Ironmak. Steelmak. (2021) 1–9, https://doi.org/10.1080/03019233.2021.1950969.
[8] H. Zhou, M. Zhou, Z. Liu, M. Cheng, K. Qiu, K. Cen, Factors controlling high-temperature zone resistance to airflow during iron ore sintering, ISIJ Int. 55 (2015) 2556–2565, https://doi.org/10.2355/isijinternational.ISIJINT-2015-311.
[9] A. Podder, Study of humidity on moisture transfer characteristics in iron ore sintering, Trans. Indian Inst. Met. 74 (2021) 1479–1487, https://doi.org/10.1007/s12666-021-02244-3.
[10] W. Yang, A. Choi, E.S. Choi, D.W. Ri, S. Kim, Combustion characteristics in an iron ore sintering bed - evaluation of fuel substitution, Combust. Flame 145 (2006) 447–463, https://doi.org/10.1016/j.combustflame.2006.01.005.
[11] J. Zhao, C.E. Loo, Dependence of flame front speed on iron ore sintering conditions, Miner. Process. Extr. Metall. (IMM Trans. Sect. C) 125 (2016) 165–171, https://doi.org/10.1080/03719553.2016.1166565.
[12] C.E. Loo, N. Tame, G.C. Penny, Effect of iron ores and sintering conditions on flame front properties, ISIJ Int. 52 (2012) 967–976, https://doi.org/10.2355/isijinternational.52.967.
[13] C.E. Loo, J. Heikkinen, Structural transformation of beds during iron ore sintering, ISIJ Int. 52 (2012) 2158–2167, https://doi.org/10.2355/isijinternational.52.2158.
[14] S. Yang, M. Zhou, W. Tang, T. Jiang, X. Xue, W. Zhang, Influence of coke ratio on the sintering behavior of high-chromium vanadium-titanium magnetite, Minerals 7 (2017), https://doi.org/10.3390/min7070107.
[15] H. Zhou, Z. Liu, M. Cheng, M. Zhou, R. Liu, Influence of coke combustion on NOx emission during iron ore sintering, Energy Fuel. 29 (2015) 974–984, https://doi.org/10.1021/ef502524y.
[16] H.Y. Ma, W. Pan, L. Liu, Z.D. Zhang, C.L. Wang, Effects of particle size of coke on iron ore sintering process, in: T. Jiang, J.Y. Hwang, D. Gregurek, Z. Peng, J. P. Downey, B. Zhao, O. Yucel, E. Keskinkilic, R. Padilla (Eds.), 10th International Symposium on High-Temperature Metallurgical Processing, 2019, pp. 649–656, https://doi.org/10.1007/978-3-030-05955-2_61.
[17] L. Xiong, Z. Peng, F. Gu, L. Ye, L. Wang, M. Rao, Y. Zhang, G. Li, T. Jiang, Combustion behavior of granulated coke breeze in iron ore sintering, Powder Technol. 340 (2018) 131–138, https://doi.org/10.1016/j.powtec.2018.09.010.
[18] X. Fan, Y. Zhao, Z. Ji, H. Li, M. Gan, H. Zhou, X. Chen, X. Huang, New understanding about the relationship between surface ignition and low-carbon iron ore sintering performance, Process Saf. Environ. Protect. 146 (2021) 267–275, https://doi.org/10.1016/j.psep.2020.09.004.
[19] H. Ogi, T. Maeda, K.-i. Ohno, K. Kunitomo, Effect of coke breeze distribution on coke combustion rate of the quasi-particle, ISIJ Int. 55 (2015) 2550–2555, https://doi.org/10.2355/isijinternational.ISIJINT-2015-089.
[20] Z. Lai, L. Lv, H. Meng, M. Zhou, P. Ma, K. Cen, H. Zhou, Effect of coating structure of granulated quasi-fuel particles in iron ore sintering, Asia Pac. J. Chem. Eng. (2021), https://doi.org/10.1002/apj.2629.
[21] Y. Tobu, M. Nakano, T. Nakagawa, T. Nagasaka, Effect of granule structure on the combustion behavior of coke breeze for iron ore sintering, ISIJ Int. 53 (2013) 1594–1598, https://doi.org/10.2355/isijinternational.53.1594.
[22] H. Zhou, P. Ma, M. Cheng, M. Zhou, Y. Li, Effects of temperature and circulating flue gas components on combustion and NOx emissions characteristics of four types quasi-particles in iron ore sintering process, ISIJ Int. 58 (2018) 1650–1658, https://doi.org/10.2355/isijinternational.ISIJINT-2018-185.
[23] H. Zhou, P. Ma, M. Zhou, Z. Lai, M. Cheng, Experimental investigation on the conversion of fuel-N to NOx of quasi-particle in flue gas recirculation sintering process, J. Energy Inst. 92 (2019) 1476–1486, https://doi.org/10.1016/j.joei.2018.08.003.
[24] K. Katayama, S. Kasama, Influence of lime coating coke on NOx concentration in sintering process, ISIJ Int. 56 (2016) 1563–1569, https://doi.org/10.2355/isijinternational.ISIJINT-2015-742.
[25] L. Ye, Z. Peng, L. Wang, A. Anzulevich, I. Bychkov, D. Kalganov, H. Tang, M. Rao, G. Li, T. Jiang, Use of biochar for sustainable ferrous metallurgy, JOM (J. Occup. Med.) 71 (2019) 3931–3940, https://doi.org/10.1007/s11837-019-03766-4.
[26] H. Purwanto, A.N. Rozhan, A.S. Mohamad, A. Zakiyuddin, Characteristics of iron ore sinter with EFB addition, IOP Conf. Ser. Mater. Sci. Eng. (2018) 342, https://doi.org/10.1088/1757-899x/342/1/012055.
[27] J. Zhao, C.E. Loo, J. Yuan, F. Wang, J. Wang, H. Zhang, H. Miao, A fundamental study of the cocombustion of coke and charcoal during iron ore sintering, Energy Fuel. 32 (2018) 8743–8759, https://doi.org/10.1021/acs.energyfuels.8b00939.
[28] C. Liu, Y.-z. Zhang, K. Zhao, H.-w. Xing, Y. Kang, Modified biomass fuel instead of coke for iron ore sintering, Ironmak. Steelmak. 47 (2018) 188–194, https://doi.org/10.1080/03019233.2018.1507070.
[29] H. Zhou, M. Zhou, P. Ma, M. Cheng, Experimental investigation on the flame front resistance of gas channel growth with melt formation in iron ore sinter beds, Proc. Combust. Inst. 37 (2019) 4607–4615, https://doi.org/10.1016/j.proci.2018.09.027.
[30] V. Shatokha, I. Korobeynikov, E. Maire, L. Gremillard, J. Adrien, Iron ore sinter porosity characterisation with application of 3D X-ray tomography, Ironmak. Steelmak. 37 (2010) 313–319, https://doi.org/10.1179/030192310x12683045805865.
[31] K.S. Augusto, S. Paciornik, Porosity characterization of iron ore pellets by X-ray microtomography, Materials Res.Ibero-Am. J. Mater. 21 (2018), https://doi.org/10.1590/1980-5373-mr-2017-0621.
[32] J. Han, W. Sun, G. Pan, In situ dynamic XCT imaging of the microstructure evolution of cement mortar in accelerated carbonation reaction, Mag. Concr. Res. 64 (2012) 1025–1031, https://doi.org/10.1680/macr.11.00173.
[33] S.C. Garcea, Y. Wang, P.J. Withers, X-ray computed tomography of polymer composites, Compos. Sci. Technol. 156 (2018) 305–319, https://doi.org/10.1016/j.compscitech.2017.10.023.
[34] K. Nushiro, N. Oyama, K. Igawa, Analysis of pore combination in sintering by hot stage X-ray computerized tomographic scanner, ISIJ Int. 39 (1999) 1239–1244, https://doi.org/10.2355/isijinternational.39.1239.
[35] M. Zhou, J. Xu, H. Zhou, Evaluating the permeability properties of green bed in iron ore sintering using high resolution X-ray computed tomography and orthogonal array tests, Powder Technol. 375 (2020) 360–368, https://doi.org/10.1016/j.powtec.2020.08.007.
[36] H. Zhou, M. Zhou, M. Cheng, W. Guo, K. Cen, Experimental study and X-ray microtomography based CFD simulation for the characterization of pressure drop in sinter bed, Appl. Therm. Eng. 112 (2017) 811–819, https://doi.org/10.1016/j.applthermaleng.2016.10.123.
[37] H. Zhou, M. Zhou, M. Cheng, X. Guo, Y. Li, P. Ma, K. Cen, High resolution X-ray microtomography for the characterization of pore structure and effective thermal conductivity of iron ore sinter, Appl. Therm. Eng. 127 (2017) 508–516, https://doi.org/10.1016/j.applthermaleng.2017.08.051.
[38] M.X. Zhou, H. Zhou, Evaluation of granule structure and strength properties of green packed beds in iron ore sintering using high-resolution X-ray tomography and uniaxial compression testing, Particuology 57 (2021) 157–166, https://doi.org/10.1016/j.partic.2020.12.005.
[39] M. Zhou, H. Zhou, Experimental investigation and numerical modeling of strength properties of iron ore sinter based on pilot-scale pot tests and X-ray computed tomography, J. Mater. Res. Technol. 9 (2020) 13106–13117, https://doi.org/10.1016/j.jmrt.2020.09.054.
[40] M. Zhou, H. Zhou, P. Ma, J. Xu, Effect of coke rate and basicity on computed tomography-measured pore parameters and effective thermal conductivity of iron ore sinter, J. Mater. Res. Technol. 8 (2019) 6191–6201, https://doi.org/10.1016/j.jmrt.2019.10.013.
[41] H. Zhou, M. Cheng, Z. Liu, M. Zhou, R. Liu, K. Cen, The relationship between sinter mix composition and flame front properties by a novel experimental approach, Combust. Sci. Technol. 190 (2017) 721–739, https://doi.org/10.1080/00102202.2017.1407316.
[42] C.E. Loo, W. Leung, Factors influencing the bonding phase structure of iron ore sinters, ISIJ Int. 43 (2003) 1393–1402, https://doi.org/10.2355/isijinternational.43.1393.